POLITECNICO
MILANO 1863

SCUOLA DI INGEGNERIA INDUSTRIALE
E DELL'INFORMAZIONE

EXECUTIVE SUMMARY OF THE THESIS

Failure Analysis on the collapse of a power transmission line by use of FEA

TESI MAGISTRALE IN MECHANICAL ENGINEERING – INGEGNERIA MECCANICA

AUTHOR: GIACOMO VETTORETTO

ADVISORS: STEFANO BERETTA, CHRISTIAN AFFOLTER, ZONGCHEN LI

ACADEMIC YEAR: 2020-2021

1. Introduction

On October 29, 2018, one among the masts part of the high-voltage power transmission line in *AlbulaPass*, Switzerland, collapsed due to an extreme windstorm event, causing a cascade sequence on other three elements of the latter.

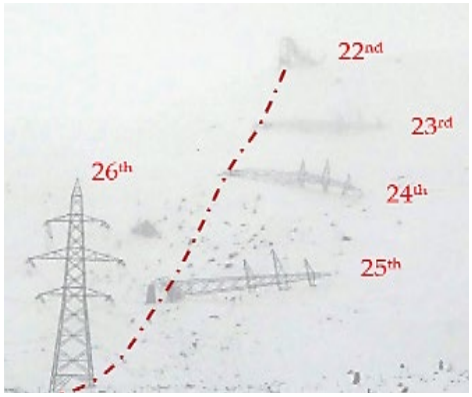

Figure 1: Towers from n22 to n26 after the storm, 2018 (source SwissGrid). Marked in red, the line path, towers n22 to n25 fallen in the perpendicular direction, n22 failed at midheight, the others at the basement; n26 still intact.

The study hereby reported discusses about the effective and reliable modeling of both the lattice towers and the line as a whole, with the purposes of estimating the load-bearing capacity, identifying possible failure positions, and replicating the dynamics of the event.
To accomplish that, *Finite Element Analysis (FEA)* was employed via the software *Abaqus CAE 2021* [1] and different analysis procedures and modeling strategies have been investigated with the purpose of better simulating structural instabilities both in simple and complex structures.
An imperfection sensitivity on the single tower model has been performed, under reasonable load assumptions and aiming to detect possible unfavorable failure modes and load-bearing capacity.
Ultimately, possible cascade dynamics of the entire line have been proposed and analyzed, and the shortcomings of the proposed approaches have been discussed.

2. Finite Element procedures

The *Abaqus CAE* offers different possibilities of analysis procedures and it is relevant to understand the strength and weaknesses of each and ultimately choose the most adequate for our final purpose:

- *Linear Buckling Analysis (LBA):* it is based on the structural linearity theory (small displacements, linear elastic material, definite

stiffness matrix), the solution is the series of eigenvalues of the introduced perturbations that make the system unstable (when stiffness matrix equals zero). However, it does not mean that the ultimate load of the structure is always the one that causes instability.

- *General, Static* and *Dynamic, Implicit*: an implicit solver finds the new increment's solution from a function of both the current and new state, resulting in a coupled system of equations that requires iterative methods (such as Newton-Raphson's) to compute a solution. The method allows for large increments, which could miss high-frequency dynamics.
- *General, RIKS*: the increment is *Arc length* based (also called *Arc-Length method*), which uses the length of the path between two increments in the force - displacement curve, decoupling the proportionality and direction of the force and displacement increase (Figure 2), similarly to a *pushover analysis*. Thus, this approach is able to overcome the instability point and show the post-bifurcation behavior.

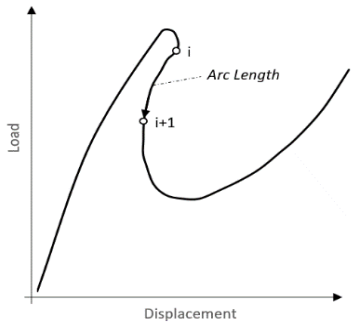

Figure 2: Arc- length increment displayed in a typical force - displacement curve.

In the study, *LBA* is adopted as a first hint on the ultimate load, then used to introduce model imperfections for a complete *RIKS* analysis, as the purpose is to estimate the actual load-bearing capacity and simulate the post-instability behavior.

3. Best practices for FEA of structural instabilities

Especially in the modeling of large structures, a tradeoff between model detail and complexity (directly proportional to computational effort) is necessary. As geometric non-linearities (large displacements) are already included by default in most analysis procedures of *Abaqus CAE*, material non-linearities, element types and mesh size have been compared on a simple L-section pinned-fixed column model to find an optimal that suits the analysis.
Empa [2] provided the material engineering curve from material testing. The following models have been analyzed:

- *Linear elastic* (with Young's modulus of 210GPa, Poisson's ratio of 0.3)
- *Bi-linear* (with a yield strength of 420MPa)
- *Non-linear* (true stress-strain characteristics)

The results show that there is negligible difference (less than 0.5%) between the *Bi-linear* and *Non-linear* models. A Bi-linear model is enough to show the material non-linearity effects and section yielding in the elastic and inelastic buckling areas.
3D, Shell and *Beam* element types have been compared with different mesh sizes. Only with fine mesh *3D* or *Shell* elements, the local buckling of the flanges can be properly displayed. Furthermore, the Beam elements do not show any buckling mode other than *flexural*, while the other element types display *torsional* and *flexural-torsional*.
At least 3-4 elements per flange and 3 in thickness are necessary to reliably simulate buckling.

4. Model experimental validation

Therefore, validation experiments are a necessary step to support a FE model accuracy. However, in most experimental setups the end-restrains condition and the initial assumption to model imperfections are very simplified.
Based on Kettler, et al. [3] experimental results, 3D models have been validated, accounting for geometric imperfections. An example is herein reported.
An L80x8 beam of length 3.17m is pinned between two clamped gusset plates via single bolt connection. The beam was modeled with *bi-linear* elastic material with elastic modulus of 210 GPa and yield limit of 333.9 MPa, gusset plate and bolts as a simple *linear elastic*, as in [3]. The bolt connection is designed according to *Eurocode 1993-1.8 [4]*. The measured beam imperfection was $e_{imp}=L/2918$.
To match the experimental data, different models with different imperfection magnitude (and direction) and friction coefficient were considered:

- *Standard* $e_{imp}=L/300$, *f=0.25: as in* [3];

- *Reduced imperfections e_{imp}=L/1350, f=0.25;*
- *Multiple mode imperfections and increased friction e_{imp}=L/400, f=0.4;*

The numerical results show lower axial stiffness in (Figure 3), but the deflection in the failure direction is well-matched, undergoing the same failure mode (Figure 7). The single bolt connection slips with friction coefficient *f*=0.25, the model with increased friction (in red) better reproduces the experiment.

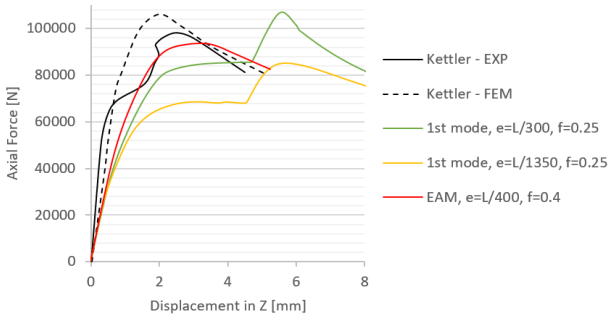

Figure 3: Axial force – displacement curves of the FE models compared to the experiments [3].

The models showed a large scatter in the load capacity estimation (between +8.6% and -13.7%), largely dependent on the type and magnitude of imperfections. The lower initial imperfection gives the lower capacity, due to the superimposed buckling mode being in the opposite direction to the actual failure. Moreover, the models are also compared with analytical buckling formulas (*Euler*, *Secant*) and *Eurocode* standards (1993-1.1 [5], 1993-3.1 [6]). The latter overestimated the experimental results by a factor between 7% and 15%.

5. Boundary conditions modeling

Structural instabilities are by definition sensitive to boundary conditions. In a lattice structure, the members are connected among each other, thus the load sharing and the flexibility of the joints is of extreme importance.
Kettler, et al. [7] introduced a systematic procedure to model and validate the end-restrain flexibility (Figure 4), effectively replacing the 3D-ends:

1. Calibration of the FE model with geometric imperfections with experimental tests.
2. Development of equivalent restrains' stiffness function (Figure 5) by applying the forcing in every degree of freedom to the FE end model.
3. Application of the stiffness functions to the *"connectors"* at the beam-ends; validation of the model by comparison with experimental tests and complete geometry FE results.

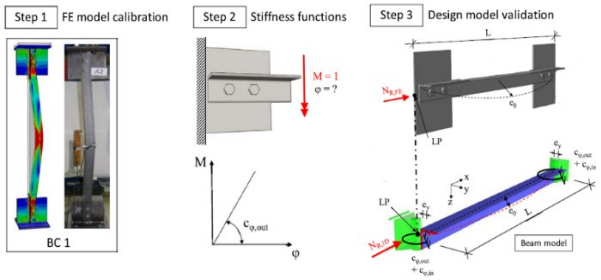

Figure 4: Ultimate load comparison with analytical formulas and standards [7].

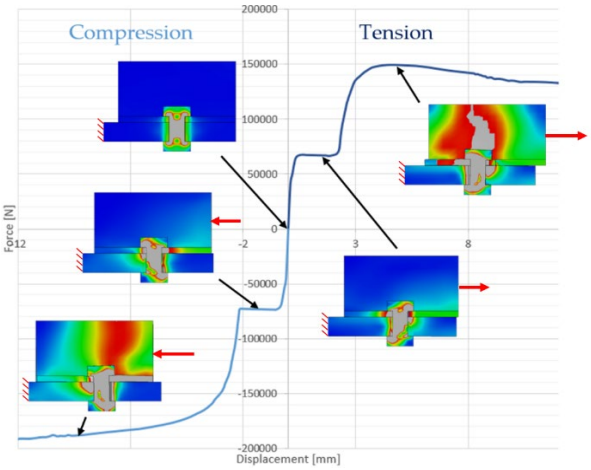

Figure 5: Stiffness functions for tension and compression in a single bolt joint.

The stiffness has been applied to a connector model that simulates what happens at the beam-ends, in the following ways:

- *Linear: initial linear stiffness coefficient;*
- *Non-linear: complete force-displacement curve / stiffness function (as in Figure 5);*
- *Rigid: fixed, fully compliant;*
- *Rigid+Free: with the only free rotational degree of freedom around the bolt axis.*

There are three main limitations to this approach: local deformations close to the joint are misrepresented; multiaxial loading cannot be properly simulated by mere uniaxial stiffness functions; no time-dependent effect, such as dynamic friction or damping.
The strategy has been applied to a single brace experiment (same as in Section 4), to a planar sub-assembly and to a 3D sub-assembly.

5.1. Brace

The brace model was modeled with *Shell* elements and compared to the 3D reference.

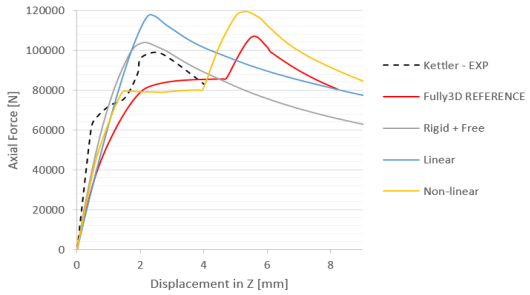

Figure 6: Axial force – displacement curves of the stiffness models compared to the experiment and *3D FE* [3].

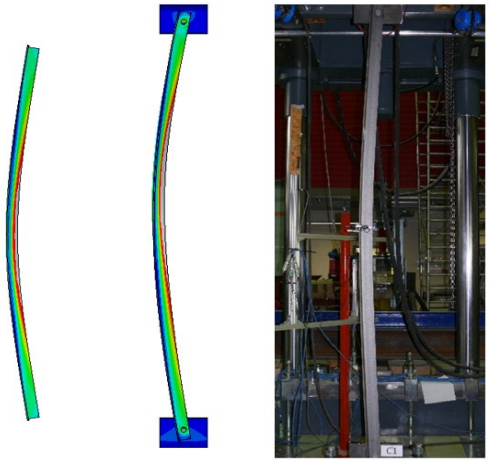

Figure 7: Comparison of the deformed state upon instability with the 3D FE reference and the real counterpart [3].

The load-displacement curve (Figure 6) well shows the slippage of the joints in the 3D and non-linear stiffness model. In all the analyzed cases, the failure mode is similar to the reference and the real counterpart, showing at least a fair level of accuracy (Figure 7).
Notice how, even though they do not display the entirety of the behavior, the *Rigid+Free* or *Linear* models are in line with the others in terms of ultimate capacity.

5.2. Planar Subassembly

Similar to a tower section face, single bolt connections have been placed in the horizontal braces (*Beam* elements) and double for the diagonals (*Beam* elements) when attached to the main legs (*Shell* elements).

Dimensions and appearance in Figure 8.

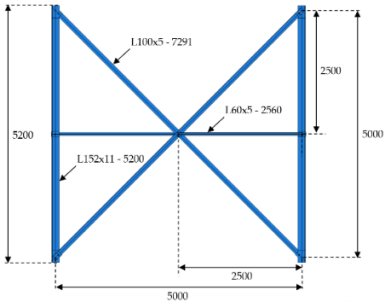

Figure 8: Dimensions of the planar sub-assembly.

None of the models has shown evidence of joint slippage. The load – displacement curve, in fact, does not have a large deviation among the different connector models: the buckling is in fact localized in the main legs, thus limiting the load sharing through the joints.

5.3. 3D Subassembly

It is a model of a tower segment, with similar geometry to the planar model (Figure 9).
However, in this case, it was not possible to have a 3D reference, due to assembly constraints, hence the modeling strategies have just been commented on.

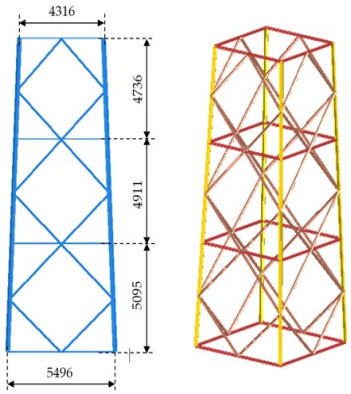

Figure 9: Dimensions of the 3D sub-assembly.

The difference between the models with rigid joints and the ones with connector stiffness is now more marked. There is also a minor difference between the *Linear* and the *Non-linear*, a sign that the slip does not affect the ultimate load capacity.

6. Towers analysis and load capacity estimation

Having perfected the approach to structural analysis for frame structures in the past Sections, it

has been employed in the modeling of the failure case initially presented.
In order to be conservative according to failure analysis, the *Shell+Beam* model with rigid connections was chosen, as it has consistently overestimated the results in Section 5.
As there was no kind of measurement system in place, nor there is no possibility of a reliable *CFD* simulation being located in a mountainous area (too many variables in play), the wind load had to be estimated from the current standards or by using experimental data.

6.1. Wind load

Most European and Swiss standards for lattice transmission towers design employ a formulation based on base wind pressure (from time-averaged measurements). These values can be found in weather maps such as the ones in *SIA 261/1* [8] (Figure 10).

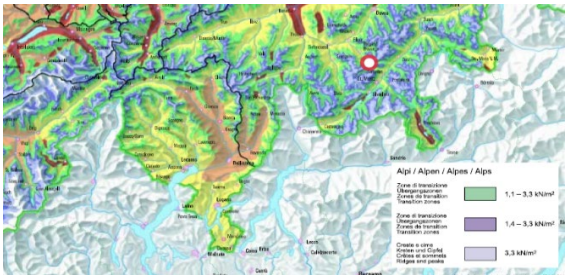

Figure 10: *SIA 261/1, appendix E* wind pressure map, *Albula Pass* highlighted [10].

The wind pressure is function of the height and can be applied on a level-based subdivision of the structure with the following formulation (based on Figure 11):

$$F_i = Q_{1,i} \cdot (1 + \alpha_i) \cdot A_{p,i} \quad (1)$$

Where F is the force applied to the level i, Q_1 the base pressure, α the shielding factor and A_p the projected surface area of the level.
As opposed to this method, one based on the forces on individual braces has been attempted, by using experimentally derived drag and lift coefficients:

$$F_{D,i} = C_D(\alpha_{1,i}) \cdot A_{nom,i} \cdot Q_{1,i} \cdot \cos^2(\alpha_{m,i}) \quad (2)$$

$$F_{L,i} = C_L(\alpha_{1,i}) \cdot A_{nom,i} \cdot Q_{1,i} \cdot \cos^2(\alpha_{m,i}) \quad (3)$$

Where F_D is the drag force in wind direction, F_L is the lift force transverse to the wind, α_m is the angle between the wind and the member axis normal plane, α_1 is the angle to the reference wind facing position in the normal plane and A_{nom} the nominal area (section width times length) of the element i.

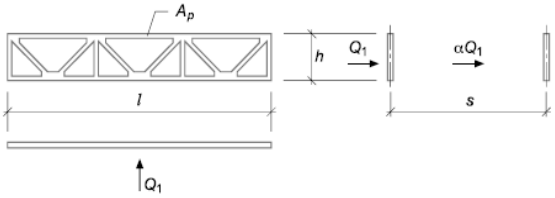

Figure 11: Force application method [8].

Different standards and the experimentally derived model have been compared level-wise in Figure 12 and as total force in the polar plots of Figure 13.

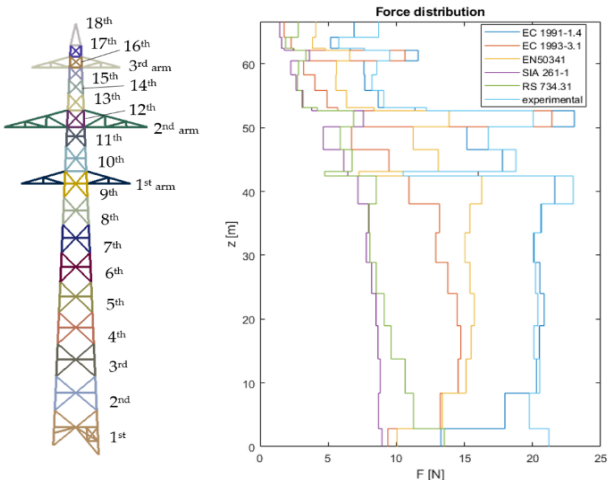

Figure 12: Forces per level height, with purely transverse wind (0°).

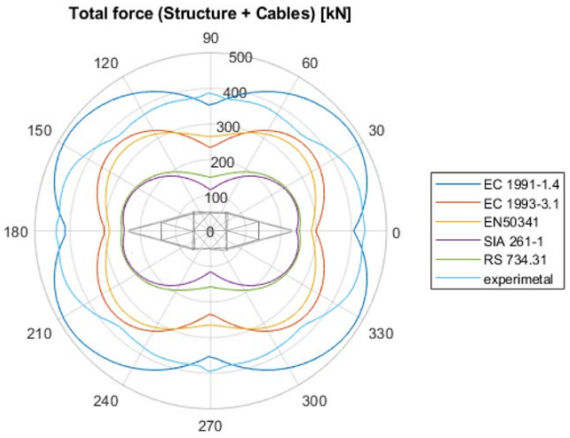

Figure 13: Total forces according to wind models.

The maximum total force is located between 20° and 45° to the line transverse direction.
As it was the least conservative with respect to the other estimates, *SIA 261/1* was the one chosen for further analysis.

6.2. Linear Buckling Analysis (LBA)

The initial *LBA* on the tower is performed in order to localize potential failure points on the structure and provide buckling imperfections. As it is a quicker and more practical procedure, it is suited for finding which wind direction is the most unfavorable for the structure, even though it does not provide the ultimate load capacity of the structure, but only the onset of instability. By creating a series of load cases in *MatLab* [9] and via setting up an *Abaqus Macro* [1] function that iteratively copies the model, different wind directions and magnitudes were analyzed. The result from this analysis is displayed as a utilization factor (instability load over the reference *SIA 261/1*) in the polar plot in Figure 14. The unfavorable wind directions are between 10° and 25° to the transverse direction and the wind load in that direction could reach the instability load according to LBA (utilization over 1). The failure mode is always focused between the 7th and 8th or in the 2nd level of the tower, (Figure 15, reference Figure 16 for level numbering).

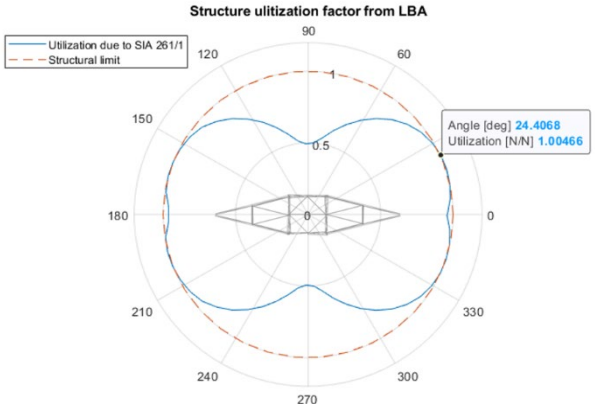

Figure 14: Instability load from LBA, in terms of utilization, highlighted 1.04 at 24.4°.

6.3. Pushover analysis (RIKS)

As pointed out by the previous Section 4 and 5, the sensitivity to imperfections can significantly affect the load-bearing capacity of the structure.
Based on literature, different imperfection modes, such as buckling imperfections superposition, missing structural elements, deformation of the supports, cable load unbalance, have been applied.
A *pushover* analysis, based on the purely transverse wind case (0°) has been performed, proportionally increasing the load magnitude to estimate maximum load-bearing capacity.

The resulting failure modes are similar to what was already evident in the *LBA* (Figure 15), but the ultimate load is in general higher than the reference (between 1.04 and 1.36 times). The most unfavorable imperfection appears to be the displacement of one basement leg.

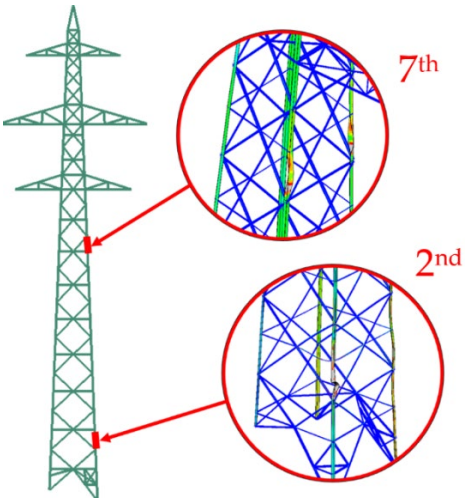

Figure 15: Failure at 7th and 2nd level displayed next to the tower.

Imperfection mode	Load capacity [applied/ref %]	Failure [level n.]
Buckling mode on 7th	132%	7th
Buckling mode on 2nd	123%	2nd
Missing e. at 5th level	135%	7th
Missing e. at the base	122%	2nd
Support displacem. 1	**104%**	2nd
Support displacem. 2	119%	2nd
Load unbalance long.	136%	7th
Load unbalance tors.	117%	2nd

Table 1: Ultimate load capacity from RIKS analysis.

The failure is inelastic buckling driven: only a small portion of the section is plasticized when the ultimate load is reached.

6.4. Post-buckling analysis

In order to obtain an estimation of the remaining capacity after the first failure, a *pushover* analysis has been carried out in a model in which the 7th or the 2nd level failed elements are removed.
In the first case, the tower's wind load capacity is reduced of 87.4%, while in the latter the tower is not even able to withstand its own weight. The tower's sudden collapse after the first elements

have failed is therefore plausible. Moreover, the damage remains localized (Figure 16).

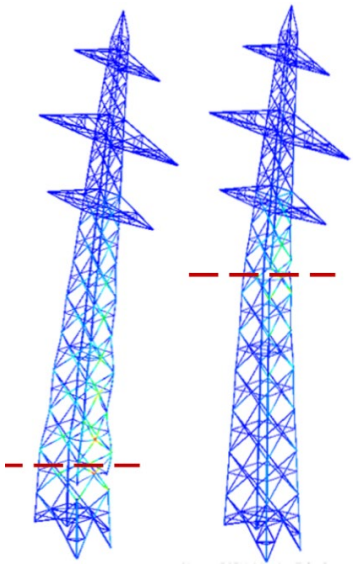

Figure 16: Post-buckling deformation with failure at 2nd (left) and 7th (left) level displayed.

7. Line analysis

Under the same load case (wind perfectly transverse to the line), two possible line failure modes can occur:

- *Cascade effect*: line collapse due to dynamic load on the neighboring towers' through the conductors, measuring the overload at cable connectors on the rest of the line.
- *Sequence of collapses:* in a separate occasion with respect to the first, due to reduction in load-bearing capacity caused by conductor force unbalance with a tower on the ground.

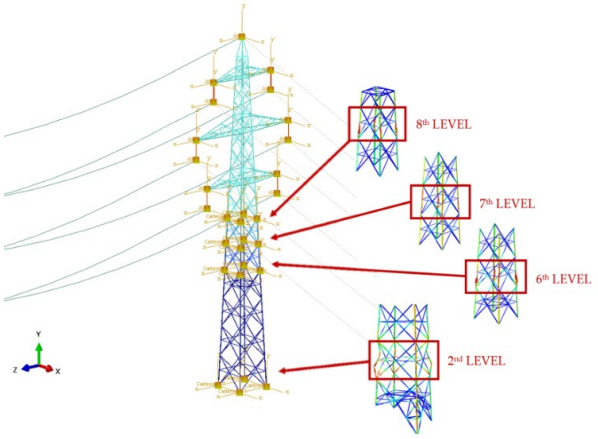

Figure 17: Example of connector subdivision, with possible section separation in three points at midheight and one at the basement.

In order to simulate the failure of the elements, the model was subdivided into core levels and attached with connector elements, to which failure load is set based on the ultimate load capacity of the above level (Figure 17).

7.1. Cascade hypothesis

The loading that passes through the cables is dissipated through the whole line, thus, it is important to look at the insulator connector points forces (arm tips of the tower) during the fall.
Several cases with each of the fallen towers starting the cascade have been simulated with a *Dynamic, Implicit* procedure, but the load increase with respect to the reference is enough to make the neighboring towers fall in the same pattern as in Figure 1: Towers from n22 to n26 after the storm, 2018 (source SwissGrid). Marked in red, the line path, towers n22 to n25 fallen in the perpendicular direction, n22 failed at midheight, the others at the basement; n26 still intact.Figure 1, no matter the failure mode or which tower collapses first.

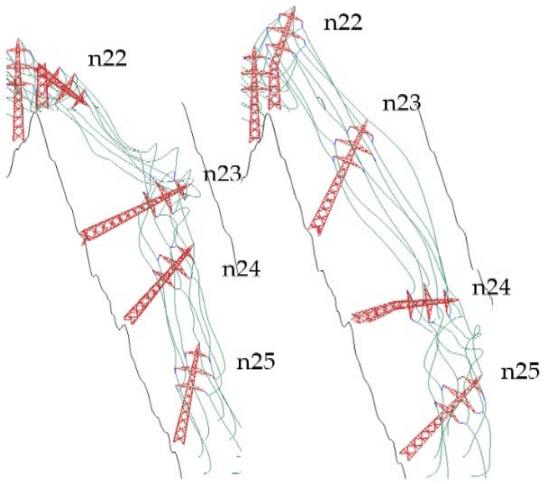

Figure 18: Examples in which tower n22 is the first to collapse (left) versus when n24 is (right).

7.2. Sequence hypothesis

The cases when the towers n22, n23 and n24 were quasi-statically brought on the ground have been analyzed, in order to measure the load unbalance on the neighboring structures, with and without wind.
Towers n24 and n23 are subjected to a high rise in the transverse and longitudinal directions. The two would most certainly fail in lower wind conditions than the analyzed so far.

8. Conclusions

The study proposes modeling methods for lattice towers under wind loading and affected by structural instability, with the final purpose of being applied to a failure analysis case.
The analysis proved to be inconclusive in terms of finding the origin of the collapse, but it proved that the wind only can cause such failure and that the towers were actually close to their ultimate capacity even under a conservative (failure analysis-wise) static load case. Moreover, the critical structural elements have been correctly identified.
The dynamics of the event has been simulated starting from different assumptions and the results hint that a cascade effect is highly probable, no matter what tower fails first.
In general, the following conclusions can be drawn:

- The main difficulties in modeling for structural instabilities are the correct simulation of boundary conditions, the more detailed consideration of imperfections (magnitude and direction are key variables) and the right use of element size and type.
- Joint flexibility affects both the single beam and lattice structure ultimate load. The pinned joint connection often employed in the design phase is not a correct representation and leads both to underestimation of single-member capacity and to incorrect failure mode prediction. The modeling with fixed elements can be a more realistic representation in some cases, but it is based on the ideal assumption of infinite moment transmission through the joints. A good solution could be the modeling via stiffness functions or coefficients, but it requires a large number of parameters and modeling detail, based on several 3D sub-models simulations.
- The margin with respect to the reference load case was of the order of 30% in all of the towers, thus it is not possible to locate the origin of the collapse. Moreover, the high sensitivity on the applied imperfections causes the ultimate load capacity can range from 104% to 136% of the reference, thus any difference in margin smaller than this range could not be undebatable evidence.
- The line dynamic simulations proved that any of the tower initially collapsing could have started a cascade effect and that all the towers (except for maybe n25) are greatly compromised in terms of load-bearing capacity if they survive the initial fall (in a collapse sequence).

References

[1] *ABAQUS 2021 Analysis User's Manual*. Simulia, Providence, RI (USA). 2021.
[2] "Material tests on samples from the failed masts No. 22-25 (tensile tests and notched impact bending tests)," Empa, 5214,020,451, 2019.
[3] M. Kettler, G. Lichtl, and H. Unterweger, "Experimental tests on bolted steel angles in compression with varying end supports," *J. Constr. Steel Res.*, vol. 155, pp. 301-315, 2019, doi: 10.1016/j.jcsr.2018.12.030.
[4] *EN 1993-1-8 (2005) (English): Eurocode 3: Design of steel structures - Part 1-8: Design of joints.*
[5] *EN 1993-1-1 (2005) (English): Eurocode 3: Design of steel structures - Part 1-1: General rules and rules for buildings.*
[6] *EN 1993-3-1 (2006) (English): Eurocode 3: Design of steel structures - Part 3-1: Towers, masts and chimneys – Towers and masts.*
[7] M. Kettler, H. Unterweger, and P. Zauchner, "Design model for bolted angle members in compression including joint stiffness," (in English), *J. Constr. Steel Res.*, Article vol. 184, 2021, Art no. 106778, doi: 10.1016/j.jcsr.2021.106778.
[8] *SIA 261/1:2003, Actions on Structures – Supplementary Specifications, Herausgeber Schweizerischer Ingenieur- und Architektenverein Postfach, CH-8039 Zürich.*
[9] MATLAB, *version 9.9 (R2020b)*. The MathWorks Inc., Natick, Massachusetts, 2020.